Computer Simulation of Defects and Oxygen Transport in Yttria-Stabilized Zirconia

R. Devanathan[a], W. J. Weber[a], S. C. Singhal[a], J. D. Gale[b]

[a]Pacific Northwest National Laboratory, P.O. Box 999, Richland, WA 99352, USA

[b]Nanochemistry Research Institute, Department of Applied Chemistry, Curtin University

of Technology, P.O. Box U1987, Perth 6845, Western Australia

Abstract

We have used molecular dynamics simulations and energy minimization calculations to examine defect energetics and oxygen diffusion in yttria-stabilized zirconia (YSZ). Oxygen vacancies prefer to be second nearest neighbors to yttrium dopants. The oxygen diffusion coefficient shows a peak at 8 mole % yttria consistent with experimental findings. The activation energy for oxygen diffusion varies from 0.6 to 1.0 eV depending on the yttria content. The $Y'_{Zr} - V^{..}_{O} - Y'_{Zr}$ complex with a binding energy of -0.85 eV may play an important role in any conductivity degradation of YSZ.

Corresponding author: Ram Devanathan
                             MS K8-93, 3335 Q Avenue
                             Pacific Northwest National Laboratory
                             Richland, WA 99352, USA
                             Phone: 509-376-7107   Fax: 509-376-5106
                             Email: ram.devanathan@pnl.gov

1. Introduction

Solid oxide fuel cells (SOFC) are attractive candidates for distributed power generation because of their high efficiency, fuel flexibility, low emissions, and modularity [1]. An important focus of current SOFC research is to improve reliability and heat management, and reduce cost by lowering the operating temperature below 700 °C using novel electrolyte and electrode materials. In order to achieve these objectives, the development of new materials and an understanding of defect and diffusion processes in existing materials are needed. The most widely used electrolyte in SOFC is yttria-stabilized zirconia (YSZ). The addition of yttria to zirconia stabilizes the cubic phase down to room temperature and improves the ionic conductivity due to the formation of oxygen vacancies when the host Zr^{4+} cations are replaced by lower-valent Y^{3+} cations. It is remarkable that despite the widespread use of zirconia in fuel cells, oxygen sensors, thermal barrier coatings, cutting tools, and orthopedic implants for several decades, atomic level defect processes are not fully understood in this material and continue to be an important focus of experimental and theoretical studies.

YSZ is an attractive SOFC electrolyte because it exhibits good oxide ion conductivity over a wide range of oxygen partial pressures, is stable under oxidizing and reducing conditions, and has good elevated temperature mechanical properties [2]. The ionic conductivity of YSZ exhibits several intriguing features. It increases with dopant concentration up to about 7-8 mole % Y_2O_3 and then decreases with further increase in dopant concentration [3,4]. Ageing of YSZ at 1000 °C results in ionic conductivity degradation, which could affect long term SOFC performance at elevated temperatures [5-8]. Several explanations have been offered in the literature for the conductivity

degradation, but an understanding of this phenomenon remains elusive. Phase transformation to tetragonal zirconia, precipitation of ordered phases such as $Y_2Zr_2O_7$, formation of microdomains, segregation of yttria at the grain boundaries, formation of a glassy phase at the grain boundaries, and short-range ordering arising from the trapping of oxygen vacancies by dopant cations are some of the theories advanced to explain ageing of YSZ [7 and references therein]. Since, the atomic-level defect processes that contribute to ageing of YSZ take place on time and length scales that are not easily accessed by experiment, it is difficult to determine the exact cause of ageing from experiment alone. Realistic computer simulations are needed to augment extensive experimental studies and provide insights into atomic-level defect phenomena.

Computer simulation has been employed to examine the defect structure, first neighbor environment of the oxygen vacancy, and activation energy for oxygen vacancy diffusion in stabilized zirconia [9-23], but there are several unresolved issues. Li and Hafskjold [10] concluded that the oxygen vacancy prefers Y to Zr as its first neighbor, consistent with early x-ray absorption spectroscopy studies [24, 25]. A recent simulation by Kilo et al [20] found that oxygen vacancies in YSZ have no preference between Zr and Y as first neighbors. However, several simulations [11-18] and experiments [26, 27] indicate that oxygen vacancies prefer to be located at the second nearest neighbor position with respect to Y^{3+}. Shimojo et al [11, 12] have concluded that regardless of the site preference of oxygen vacancies, the variation of the ionic conductivity of YSZ with yttria mole % arises from reduced transition probabilities (higher migration barriers) of oxygen ions across dopant cation edges. Following on from this idea, recent kinetic Monte Carlo simulations [22, 23] have studied oxygen diffusion based on the

determination of migration barriers for different first neighbor environments using *ab initio* calculations. However, there remains considerable disagreement in the published values of the activation energy for oxygen diffusion in YSZ obtained by experiment and simulation. This points to a need to thoroughly review the existing data and perform molecular dynamics simulations of oxygen migration without the use of parameterized diffusion barriers.

Experimentally, the activation energy is determined from measurements of ionic conductivity or [18]O tracer diffusion coefficient as a function of temperature. The dc conductivity, σ, of a fast ion conductor can be written as;

$$\sigma T = A \exp(-\frac{\Delta H_a + \Delta H_m}{k_B T}),$$ (1)

where A is a pre-exponential factor, ΔH_m is the enthalpy of oxygen migration, k_B is the Boltzmann constant, and T is the absolute temperature [28]. ΔH_a is an association enthalpy that, along with the association entropy ΔS_a, determines the fraction of oxygen vacancies, f, that are not bound in clusters and are thus free to migrate as;

$$f = \exp(\frac{\Delta S_a}{k_B}) \exp(-\frac{\Delta H_a}{k_B T}).$$ (2)

ΔH_a has been determined to be about 0.1 to 0.2 eV in fully stabilized zirconia [28]. ΔH_m is determined from the tracer diffusion coefficient, D, using the expression;

$$D = D_0 \exp(-\frac{\Delta H_m}{k_B T}),$$
(3)

where D_0 is the pre-exponent. Experimental reports in the literature present $\Delta H_a + \Delta H_m$ or

ΔH_m. Comparison between different experimental data sets is not straightforward,

because the level of impurities present in the sample is not readily available. Impurities

can have an impact on the measured conductivity as well as degradation phenomena.

Experimental values of the enthalpy of migration ($\Delta H_a + \Delta H_m$ or ΔH_m) are plotted

in Fig. 1 as a function of yttria mole % and the distinction is made in the text below. The

earliest data (1970) is from Casselton [29] who measured low field dc conduction in

polycrystalline YSZ samples. In this case, the samples were fabricated from 99.99%

purity yttria and zirconia containing 2% HfO_2, 0.2% each of TiO_2 and SiO_2 and 0.02%

Fe_2O_3, and sample density was 92 to 95% of the theoretical value. Casselton's data [29]

show that $\Delta H_a + \Delta H_m$ increases almost linearly from 0.7 to 1.3 eV with yttria content from

8.5 to 20 mole %. This is completely consistent with the values of $\Delta H_a + \Delta H_m$ obtained by

Ioffe *et al* [3] following conductivity measurements from polycrystalline samples with

density nearly 97% of theoretical value and containing 0.5% each of Si and Cu and 0.1%

each of Mg and Ca. Recent ac impedance measurements from polycrystalline YSZ by

Luo *et al* [28] at temperatures between 520 and 640 K indicate that $\Delta H_a + \Delta H_m$ increases

monotonically from 1.09 to 1.26 eV for yttria content of 7.5 to 12 mole %. The two

inverted triangle data points corresponding to the polycrystalline YSZ values given by

Oishi and Ando [30] are considerably (~0.3 eV) lower than the above data. A trend at

odds with that shown by polycrystalline samples is observed in [18]O tracer diffusion

experiments in single crystal YSZ [31]. ΔH_m appears to be independent of yttria content and exhibits an average value of ~ 0.95 eV. It is remarkable that despite the differences in purity, density, and grain size of the samples examined and the different measurement techniques used over a period of 40 years, most experiments seem to agree that ΔH_m for oxygen migration in 8 to 30 mole % YSZ lies between 0.5 and 1.3 eV and that it increases with increasing yttria content.

In Fig. 2, the published values of ΔH_m in YSZ obtained from a determination of D as a function of T by computer simulation are plotted as a function of yttria content. In computer simulations, D is calculated from the mean square displacement of oxygen ions, MSD, using

$$D = \frac{MSD}{6t} \quad . \tag{4}$$

It is much more difficult to discern a trend in the simulated data than with the experimental data shown in Fig. 1. Li and Hafskjold [10] used two different interaction potentials in their molecular dynamics (MD) simulation of YSZ with a small 384 ion system and a large time step of 5 fs. With one potential (filled circles), they observed a value of about 0.2 eV for E_a more or less independent of yttria content, while with the other potential (open circles), E_a was found to rise from 0.4 to 0.8 eV with increasing yttria content from 5 to 20 mole %. MD simulations by Sawaguchi and Ogawa [19] indicate that ΔH_m increases from 0.4 to 1 eV with yttria content rising from 5 to 30 mole %. However, a more recent MD study by Kilo et al [21] has concluded that ΔH_m in YSZ

is about 0.92 eV and nearly independent of the yttria content from 6 to 24 mole %. Kinetic Monte simulations by Pornprasertsuk et al [23], based on migration barriers determined by *ab initio* calculations, show that ΔH_m increases from 0.65 to 1.0 eV for yttria concentration from 6 to 15 mole% with some difference between values obtained below 1050 K (marked low in Fig 2) and those above 1050 K (high). Due to differences in approaches and results, there is an obvious need for long time scale (1 ns or longer) simulation of oxygen migration and anion vacancy-dopant interactions in YSZ using reliable potentials. None of the available classical potentials for zirconia can correctly model the monoclinic, tetragonal and cubic phases. The potential developed by Schelling et al [17] based on the work of Zacate et al [16] appears to be the best choice for this task. It gives the tetragonal phase as the stable form, correctly models the tetragonal-to-cubic phase transition at 2000 K on heating and 1850 K on cooling, and fully stabilizes cubic zirconia at about 4 mole % yttria [17].

In the present work, we have used the potential of Schelling et al [17] to evaluate oxygen migration barriers for various distributions of Y^{3+} in the first and second neighbor shell, the energetics of oxygen vacancy-Y^{3+} interactions, and the binding energy of defect-dopant clusters. These static calculations indicate that the migration energy is influenced by ions that lie well beyond the first neighbor shell. In order to reliably include environment effects in modeling oxygen diffusion we have performed classical MD simulations and compare our results to both experiment and recent kMC simulations [22, 23]. This work also provides insights into defect-dopant interactions and conductivity degradation in YSZ.

2. Details of the simulation

We used the potential of Schelling et al [17] with the DL_POLY code [33] (version 2.14) to perform molecular dynamics (MD) simulations, and the GULP code [32] to perform energy minimization and determine oxygen migration barrier heights in YSZ in a variety of first and second neighbor environments. This potential model uses formal charges for the ions, and short-range Buckingham potentials in addition to the Coulombic interaction.

The MD simulation cell consisted of 5x5x5 unit cells with periodic boundary conditions, a constant temperature and zero external pressure (constant NPT ensemble). We studied seven different compositions, namely 5.93, 7.99, 9.89, 12.11, 14.94, 17.92, and 25.0 mole % Y_2O_3, at temperatures of 1125, 1350, 1667, 2000 and 2500 K for 2 to 5 ns after initial equilibration for 0.05 ns. The cubic phase is fully stabilized for all the compositions simulated. We obtained the oxygen diffusion coefficient from the slope of the variation of mean square ionic displacement with time. We substituted specific number of Y^{3+} for Zr^{4+}, determined by the composition, at randomly chosen Zr^{4+} cation sites, and removed an O^{2-} for every two Y^{3+} from a randomly selected anion site. Since there was no cation migration during the MD simulation, our results are based on a random distribution of Y^{3+}.

The energy minimization calculations used 4x4x4 unit cells with a typical dilute yttria concentration obtained by replacing two ZrO_2 molecules by one Y_2O_3 as described below.

$$Y_2O_3 + 2Zr_{Zr}^{x} + O_O^{X} \rightarrow 2Y_{Zr}^{'} + V_O^{\cdot\cdot} + 2ZrO_2 \tag{5}$$
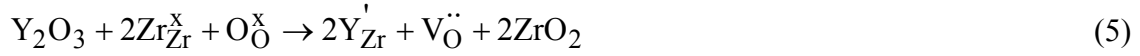
We calculated the binding energies of $Y_{Zr}^{'} \text{-} V_O^{\cdot\cdot}$ and $Y_{Zr}^{'} \text{-} Y_{Zr}^{'}$ as a function of the distance between the constituents. We determined the oxygen migration barrier by moving an oxygen ion incrementally along [001] toward an adjacent $V_O^{\cdot\cdot}$, constraining this ion to relax in the (001) plane while allowing the other ions to relax. At the saddle point, the two nearest cations that constituted the migration edge were also constrained to relax in the (001) plane as discussed by Pornprasertsuk et al [23]. By combining MD simulations with static energy minimization calculations, we were able to obtain better insights than possible with the use of just one of these methods.

3. Results

Fig. 3 shows the variation of the lattice parameter of YSZ (cubic) as a function of yttria mole % obtained in the present work by MD simulation (triangles) at 300 K and zero external pressure in the NPT ensemble for 20 ps. The simulation results agree well with the corresponding experimental values (squares) of Pascual and Duran [34] and serve to validate the potential. The coefficient of linear thermal expansion in our simulation was $6.8\text{-}8.0\text{x}10^{-6}$ K^{-1}, in reasonable agreement with the experimental value of $9.6\text{x}10^{-6}$ K^{-1} for YSZ [35].

Fig. 4 shows the radial distribution functions for Zr-O and Y-O pairs in 10 mole % YSZ at 1125 K obtained from 10 configurations during a 2 ns simulation. The trend is

similar at other compositions and temperatures examined. The average Zr-O first neighbor distance is shorter than the corresponding Y-O distance by about 0.02 nm, while the second and subsequent neighbor distributions of Zr-O and Y-O are similar. It is evident that the first neighbor environment is quite different for Zr and Y in YSZ.

Fig. 5 shows the average coordination number of Zr and Y in YSZ as a function of composition at 1350 K. Due to the presence of anion vacancies, the coordination number is less than the typical value of 8 for the cubic fluorite structure. The coordination number of Y is higher than that of Zr, which indicates that oxygen vacancies prefer not to be nearest neighbors to Y consistent with the general consensus from simulations [11-18] and experiments [26, 27]. Elegant first principles calculations by Bogicevic and Wolverton [18] have shown that this site preference is due to a delicate balance between elastic and electrostatic interactions. These authors argue that the larger radius of Y^{3+} leads to strong vacancy-Zr association that hampers ionic conduction by the vacancy mechanism.

Fig. 6 is a superposition of projections along the Y-axis of oxygen ions positions from 4000 configurations at intervals of 0.025 ps during an MD simulation of 8 mole % YSZ at 2000 K. The area shown (5x5 unit cells) was divided into 100x100 pixels and each pixel was assigned a gray scale based on the number of oxygen ions counted within that pixel. White and black represent, respectively, the extremes of high and low probability of finding an oxygen ion. Similar plots were obtained for projections along the X- and Z- axes, which indicate that the oxygen ion transport occurs along [001].

Fig. 7 is an Arrhenius plot (equation 3) of D vs. $(1/k_BT)$ for oxygen migration in 6, 8 and 10 mole % YSZ. The data points are from the present MD simulations for a period

of 2 to 5 ns at 1125, 1350, 1667, 2000 and 2500 K. The lines are the best fit to the data according to equation 3. The slope gives the activation energy for oxygen migration, and the intercept the pre-exponent. We find that the diffusion coefficient is highest at 8 mole % YSZ, consistent with experimental results [3,4]. The data points for 12, 15, 18 and 25 mole % Y_2O_3 are not shown for the sake of clarity. Above 10 mole % Y_2O_3, the diffusion coefficient decreased with increasing yttria content.

The activation energy for oxygen migration in YSZ is shown as a function of composition in Fig. 8. The plot is on the same scale as Fig. 1 and 2 to facilitate comparison with published data. The activation energy (ΔH_m) shows an upward trend with increasing Y_2O_3 content. The best linear fit is also shown and has the form;

$$\Delta H_m \, (eV) = 0.5 + 0.02y, \tag{6}$$

where y is the yttria mole % (in the range 6 to 25 %). Activation energies obtained in the present work are about 0.2 eV below the experimental data ($\Delta H_m + \Delta H_a$) of Ioffe et al [3] shown in Fig. 1. Since ΔH_a is estimated to be about 0.1-0.2 eV [28], we consider our data to be in agreement with the values of Ioffe et al [3] and the general experimental trend of increasing activation energies with increasing mole % of Y_2O_3. Our data also show good agreement with the values reported by Pornprasertsuk et al [23] based on first principles calculations.

D_0 and ΔH_m are listed in Table I along with D at a typical operating temperature (1273 K) for all the YSZ compositions studied. By determining these values using molecular dynamics, we have implicitly included ionic environment effects that are often

left out in static calculations of barrier heights that consider mainly first neighbor effects. We find that the overall trend is that both D_0 and ΔH_m increase with increasing mole % of Y_2O_3. As the Y_2O_3 content increases, the vacancy concentration increases, leading to an increase in D_0. However, the increase of D due to this effect is countered by an increase in ΔH_m. It appears that the balance between these two effects is reached at around 8 mole % YSZ as shown by the last column in Table I.

In an effort to understand these defect-dopant interactions, we have calculated, using the GULP code [32], the energetics of $Y'_{Zr} - V_O^{\cdot\cdot}$ and $Y'_{Zr} - Y'_{Zr}$ interactions as a function of separation. Fig. 9 shows the average binding energy of $Y'_{Zr} - V_O^{\cdot\cdot}$ for the first through tenth neighbor separations obtained from three configurations that differed in the relative positions of Y'_{Zr} and $V_O^{\cdot\cdot}$. There was no other Y'_{Zr} or $V_O^{\cdot\cdot}$ within 1 nm of the interacting $Y'_{Zr} - V_O^{\cdot\cdot}$. The binding energy is expected to become increasingly negative based strictly on the electrostatic effect, as the Y'_{Zr} and $V_O^{\cdot\cdot}$ approach each other from infinite separation to first neighbor distance. However, we find that the second neighbor position with respect to the dopant is the lowest energy configuration for $V_O^{\cdot\cdot}$. This has been attributed to the competing electrostatic and elastic interactions [18]. Our binding energy values of -0.28, -0.45, -0.16 and -0.04 eV, respectively, for the first, second, third and fourth neighbor separations compare favorably with corresponding values of -0.30, -0.35, -0.19 and -0.13 eV from first principles calculations [23]. It is important to note that the $Y'_{Zr} - V_O^{\cdot\cdot}$ binding energy is in excess of 0.15 eV even at the third neighbor separation. Due to strong electrostatic effect, the binding energy will be sensitive to the

environment of the defect and dopant. In a realistic electrolyte composition, such as 8 mole % YSZ, Y'_{Zr} and $V_O^{\cdot\cdot}$ present in the second through fourth neighbor shells will have an influence on the binding energy. Thus, values obtained from idealized binding energy calculations such as this can only be used as approximate guidelines to gain insights into atomic level defect processes. In this case, the occurrence of an energy minimum at the second neighbor position, consistent with first principles calculation [23], is more significant than the actual values.

Fig. 10 shows the average binding energy of Y'_{Zr}-Y'_{Zr} for the first through seventh neighbor separations obtained from three configurations. Electrostatics dictates that the energy should increase as dopants approach each other from infinite separation. However we find, analogous to the case of Y'_{Zr}-$V_O^{\cdot\cdot}$, the maximum in the binding energy occurs at the second neighbor separation of Y'_{Zr}-Y'_{Zr} instead of the first neighbor separation. The binding energies calculated in the present work, do not vary much with separation beyond the fourth neighbor distance (about 0.7 nm). Our binding energy values of 0.13, 0.18, 0.05 and 0.02 eV, respectively, for the first, second, third, and fourth neighbor separations are in general agreement with corresponding values of 0.03, 0.14, 0.00, and -0.1 eV from first principles calculations [23]. As discussed above, ionic environmental effects can modify these values, and the fact that first neighbor separation is preferred to second neighbor separation is more important than the absolute energy values.

Given the Y'_{Zr}-$V_O^{\cdot\cdot}$ and Y'_{Zr}-Y'_{Zr} binding energy trends presented above, it is pertinent to examine the oxygen migration barriers for various first neighbor cation

arrangements. Fig. 11 (a-e) shows the migration of an O^{2-} anion (large grey circle) between two adjacent cation tetrahedra along [001]. Zr^{4+} and Y^{3+} cations are represented as small white and black circles, respectively. Previous simulations had examined the migration barrier based on the identity of two cations that form the common edge between the two tetrahedra and concluded that it was highest across a Y'_{Zr} - Y'_{Zr} edge [12, 22]. Pornprasertsuk et al [23] went a step further and parameterized the migration barrier using first principles calculations for almost all possible Y and Zr distributions in the two tetrahedra.

In the present work, we evaluated the migration barrier for five representative cases shown in Fig 11 (a-e). When the tetrahedra are occupied entirely by Zr, as in Fig. 11a, we obtain ΔH_m of about 0.3 eV. This decreases to 0.2 eV when $V_O^{\cdot\cdot}$ moves from first neighbor to second neighbor with respect to Y'_{Zr} (Fig. 11b) and increases to about 0.4 eV for the opposite jump (Fig. 11c). In the above three cases, the jump was across a Zr-Zr edge. The barrier heights are 0.85 and 2.04 eV, respectively for Zr-Y (Fig. 11d) and Y-Y (Fig. 11e) edges. The ΔH_m values for Fig. 11(a-e) from first principles [23] are 0.67, 0.20, 0.80, 1.19 and 1.23, respectively. The overall trends in the migration barrier agree with the results from first principles, while the actual values are quite different. This is understandable due to differences in system size, composition, and simulation methods and inherent assumptions between these calculations. The fixed charge approximation in empirical potentials could also be a contributing factor.

In an effort to further explore the dopant-defect binding energy, we have examined a neutral Y'_{Zr} - $V_O^{\cdot\cdot}$ - Y'_{Zr} complex shown in Fig. 11f. This complex consist of

two Y'_{Zr} that are first neighbors with respect to each other and have a $V^{..}_O$ in the common second neighbor position. We have determined the binding energy of this complex to be -0.85 eV, which indicates that this complex will not dissociate easily. The formation of such a complex will reduce the fraction of freely migrating $V^{..}_O$. Butler et al [9] have also found a high binding energy of -0.63 eV for this complex. We believe that this complex may play an important role in the degradation of electrical conductivity of YSZ upon prolonged operation as discussed below.

4. Discussion

Defect interactions in YSZ are known to be dictated by a delicate balance between electrostatic and elastic effects [18]. The present work highlights the fact that electrostatic interactions between dopants and defects are not negligible even at the third neighbor distance. Therefore, parameterizing the oxygen migration energy barrier based on the cation edge between tetrahedra [22] or the first neighbor environment of the migrating oxygen ion [23] has limited validity. This has been acknowledged in previous work [22, 23], but justified on the grounds that the computational expense and complexity would become unmanageable if one were to attempt to determine the migration barriers for all possible arrangements of cations and oxygen vacancies within a radius that included third neighbors. By combining molecular dynamics simulations and energy minimization calculations using reliable empirical potentials, we have demonstrated an alternative approach to probing the atomic level mechanisms in SOFC electrolytes.

The binding energies of various defect complexes obtained in the present work reveal the strength of defect-dopant interactions in YSZ. The large negative binding energy value (-0.85 eV) for the Y'_{Zr}-$V_O^{\bullet\bullet}$-Y'_{Zr} complex provides valuable insights into possible microstructural evolution in YSZ at elevated temperature. The formation of this complex is controlled by cation migration, which is slow due to very high activation energy of 4.2 eV for Y'_{Zr} migration in YSZ [36]. The Y'_{Zr}-Y'_{Zr} cation edge that is key to the Y'_{Zr}-$V_O^{\bullet\bullet}$-Y'_{Zr} complex can form only after long term operation at high temperature. The formation of Y'_{Zr}-Y'_{Zr} pairs may be governed by the facts that first neighbor separation is preferred to second neighbor separation (Fig. 10) and Y'_{Zr} cannot remain separated at large distances from each other especially for high mole % Y_2O_3. The barrier for migration across such a cation edge is high (Fig. 11d-e) and the formation of these edges restricts the available pathways for diffusion. This argument is similar to the percolation model invoked by Meyer et al [37] to explain the anomalous conductivity of fluorite-related oxides.

Our MD simulation of oxygen migration in YSZ, along with the static migration energy barrier calculations, explain the conductivity decline at high dopant concentrations. As the yttria content increases, the vacancy concentration increases leading to an increase in the pre-exponent of the diffusion coefficient. At the same time, the increase in the number of Y'_{Zr} leads to a greater fraction of cation edges being associated with high migration energy barriers. This causes the overall activation energy for oxygen migration to increase from 0.6 to 1.0 eV as the yttria content increases from 6 to 25 mole %.

When a Y'_{Zr} - Y'_{Zr} edge captures a $V_O^{\cdot\cdot}$, a complex with a large negative binding energy results. This can lead to conductivity degradation due to decrease in the free $V_O^{\cdot\cdot}$ available for diffusion. Since these complexes exist on a length scale below 1 nm, direct observation of such complexes is a challenge in experiments. The formation of such a complex may also result in local changes in composition and lead to formation of nanoscale regions of the tetragonal phase. The present work shows that MD simulations using reliable empirical potentials can capture the essential atomistic mechanisms in YSZ. The development of such reliable potentials for other SOFC electrolytes, and the extension of these simulations to much longer time and distance scales using multiscale modeling approaches are the next steps currently being pursued in this effort.

5. Conclusions

We have used molecular dynamics simulations and static energy minimization calculations with a Buckingham-type potential to model oxygen migration and defect interactions in YSZ. The results explain the experimentally observed peak in the ionic conductivity at 8 mole % yttria. The activation energy for oxygen diffusion was found to be 0.6 to 1.0 eV for 6 to 25 mole % YSZ. The formation of Y'_{Zr} - Y'_{Zr} nearest neighbor clusters could hamper oxygen diffusion by blocking anion migration paths. The formation of the neutral Y'_{Zr} - $V_O^{\cdot\cdot}$ - Y'_{Zr} complex with a binding energy of -0.85 eV could be an important contributor to conductivity degradation of YSZ.

References

[1]   S. C. Singhal, Solid State Ionics 152-153 (2002) 405.

[2]   M. Ralph, A. C. Schoeler, and M. Krumpelt, J. Mater. Sci. 36 (2001) 1161.

[3]   A. I. Ioffe, D. S. Rutman, and S. V. Karpachov, Electrochim. Acta 23 (1978) 141.

[4]   S. P. S. Badwal, Solid State Ionics 52 (1992) 23.

[5]   F. T. Ciacchi and S. P. S. Badwal, J. European Ceram. Soc. 7 (1991) 197.

[6]   J. Kondoh, T. Kawashima, S. Kikuchi, Y. Tomii, and Y. Ito, J. Electrochem. Soc. 145 (1998) 1527.

[7]   J. Kondoh, S. Kikuchi, Y. Tomii, and Y. Ito, J. Electrochem. Soc. 145 (1998) 1536; ibid. 1550.

[8]   C. Haering, A. Roosen, and H. Schichl, Solid State Ionics 176 (2005) 253.

[9]   V. Butler, C. R. A. Catlow, and B. E. F. Fender, Solid State Ionics 5 (1981) 539.

[10]   X. Li and B. Hafskjold, J. Phys.: Condens. Matter 7 (1995) 1255.

[11]   F. Shimojo, T. Okabe, F. Tachibana, M. Kobayashi, and H. Okazaki, J. Phys. Soc. Japan 61 (1992) 2848.

[12]   F. Shimojo and H. Okazaki, J. Phys. Soc. Japan 61 (1992) 4106.

[13]   M. S. Khan, M. S. Islam, and D. R. Bates, J. Mater. Chem., 8, 2299 (1998).

[14]   Y. Yamamura, S. Kawasaki, and H. Sakai, Solid State Ionics 126 (1999) 181.

[15]   G. Stapper, M. Bernasconi, N. Nicoloso, and M. Parrinello, Phys. Rev. B 59 (1999) 797.

[16]   M. O. Zacate, L. Minervini, D. J. Bradfield, R. W. Grimes, and K. E. Sickafus, Solid State Ionics 128 (2000) 243.

[17]   P. K. Schelling, S. R. Phillpot, and D. Wolf, J. Am. Ceram. Soc. 84 (2001) 1609.

[18]   A. Bogicevic and C. Wolverton, Phys. Rev. B 67 (2003) 024106.

[19]   N. Sawaguchi and H. Ogawa, Solid State Ionics 128 (2000) 183.

[20]   M. Kilo, R. A. Jackson, and G. Borchardt, Phil. Mag. 11 (2003) 3309.

[21]   M. Kilo, C. Argirusis, G. Borchardt, and R. A. Jackson, Phys. Chem. Chem. Phys. 5 (2003) 2219.

[22]   R. Krishnamurthy, Y. G. Yoon, D. J. Srolovitz, and R. Car, J. Am. Ceram. Soc. 87 (2004) 1821.

[23]   R. Pornprasertsuk, P. Ramanarayanan, C. B. Musgrave, and F. B. Prinz, J. Appl. Phys. 98 (2005) 103513.

[24]   H. Morikawa, Y. Shimizugawa, F. Marumo, T. Harasawa, H. Ikawa, K. Tohji, and Y. Udagawa, J. Japan Ceram. Soc. 96 (1988) 253.

[25]   M. H. Tuilier, J. Dexpert-Ghys, H. Dexpert, and P. Lagarde, J. Solid State Chem. 69 (1987) 153.

[26]   C. R. A. Catlow, A. V. Chadwick, G. N. Greaves, and L. M. Moroney, J. Am. Ceram. Soc. 69 (1986) 272.

[27]   P. Li, I. W. Chen, and J. E. Penner-Hahn, Phys. Rev. B 48 (1993) 10074.

[28]   J. Luo, D. P. Almond, and R. Stevens, J. Am. Ceram. Soc. 83 (2000) 1703.

[29]   R. E. W. Casselton, Phys. Stat. Sol. A 2 (1970) 571.

[30]   Y. Oishi and K. Ando, NATO ASI Ser., Ser. B 129 (1985) 189.

[31]   M. Weller, R. Herzog, M. Kilo, G. Borchardt, S. Weber, and S. Scherrer, Solid State Ionics 175 (2004) 409.

[32]   J.D. Gale and A.L. Rohl, Mol. Simul. 29 (2003) 291.

[33]   W. Smith and T. R. Forester, J. Mol. Graphics 14 (1994) 136.

[34]   C. Pascual and P. Duran, J. Am. Ceram. Soc. 66 (1983) 23.

[35]   E. H. Kisi and C. J. Howard, Key Eng. Mater. 153-154 (1998) 1.

[36]   M. Kilo, M. A. Taylor, C. H. Argirusis, G. Borchardt, B. Lesage, S. Weber, S. Scherrer, H. Scherrer, M. Schroeder, and M. Martin, J. Appl. Phys. 94 (2003) 7547.

[37]   M. Meyer, N. Nicoloso, and V. Jaenisch, Phys. Rev. B 56 (1997) 5961.

TABLE I. Pre-exponent (D_0) and activation energy (ΔH) for oxygen diffusion in YSZ.

Mole % Y_2O_3	D_0 (10^{-9} m^2/s)	ΔH (eV)	D (m^2/s) at 1273 K
6	4.94	0.59	2.28x10-11
8	6.08	0.60	2.56x10-11
10	11.81	0.73	1.52x10-11
11	12.62	0.75	1.30x10-11
12	12.59	0.76	1.24x10-11
15	20.03	0.86	0.79x10-11
18	11.01	0.82	0.62x10-11
25	20.48	0.98	0.27x10-11

Figure captions

Fig. 1. Enthalpy of migration of oxygen in YSZ from experimental data. Lines drawn

through the data points show trends in the data.

Fig.2.. Activation energy for oxygen migration in YSZ from simulation. The data points

have been connected by lines to show trends in the data.

Fig. 3. Lattice parameter of YSZ at 300 K as a function of Y_2O_3 content.

Fig. 4. Radial distribution function of Zr-O (solid line) and Y-O (dashed line) pairs in 10

mole % YSZ at 1125 K.

Fig. 5. Average number of O neighbors for Y (▲) and Zr (o) in YSZ at 1350 K with

linear fits to the data.

Fig. 6. Projection of oxygen ion positions along [010] direction from 4000 molecular

dynamics configurations in YSZ at 2000 K. Gray levels represent the probability

of finding an oxygen from 0 (black) to 1 (white).

Fig. 7. Arrhenius plot of the diffusion coefficient as a function of reciprocal temperature

(1/T) for 6 (■), 8(▲), and 10 (♦) mole % YSZ. Linear fits to the data are also

shown.

Fig. 8. Activation energy for oxygen migration in YSZ as a function of composition

along with a linear fit to the data.

Fig. 9. Dopant-vacancy binding energy in YSZ as a function of separation. Lines

connecting the data points are shown to guide the eye.

Fig. 10. Dopant-dopant binding energy in YSZ as a function of separation. Lines

connecting the data points are shown to guide the eye.

Fig. 11. (a-e) O^{2-} (large grey circle) migration with different distributions of Zr^{4+} (small white circle) and Y^{3+} (small black circle) in the first neighbor shell; (f) $Y'_{Zr} - V_O^{\cdot\cdot} - Y'_{Zr}$ complex shown connected by solid lines. $V_O^{\cdot\cdot}$ is represented by a small grey square.
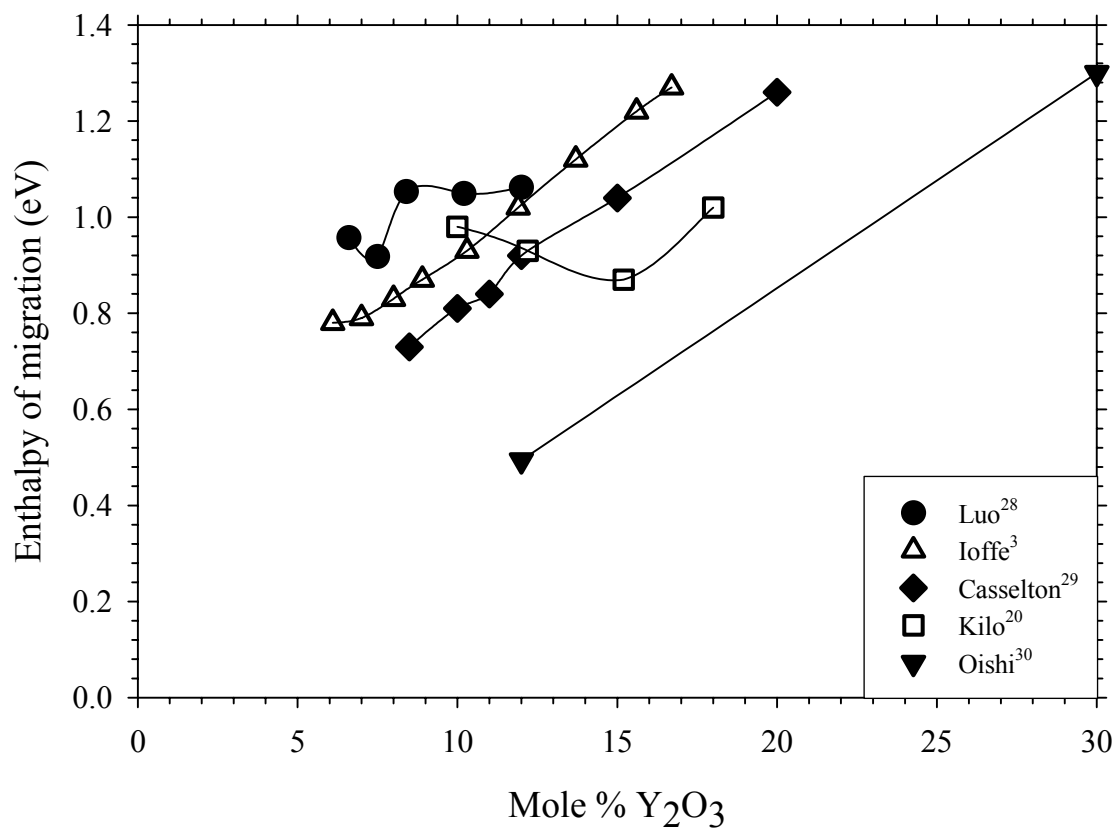
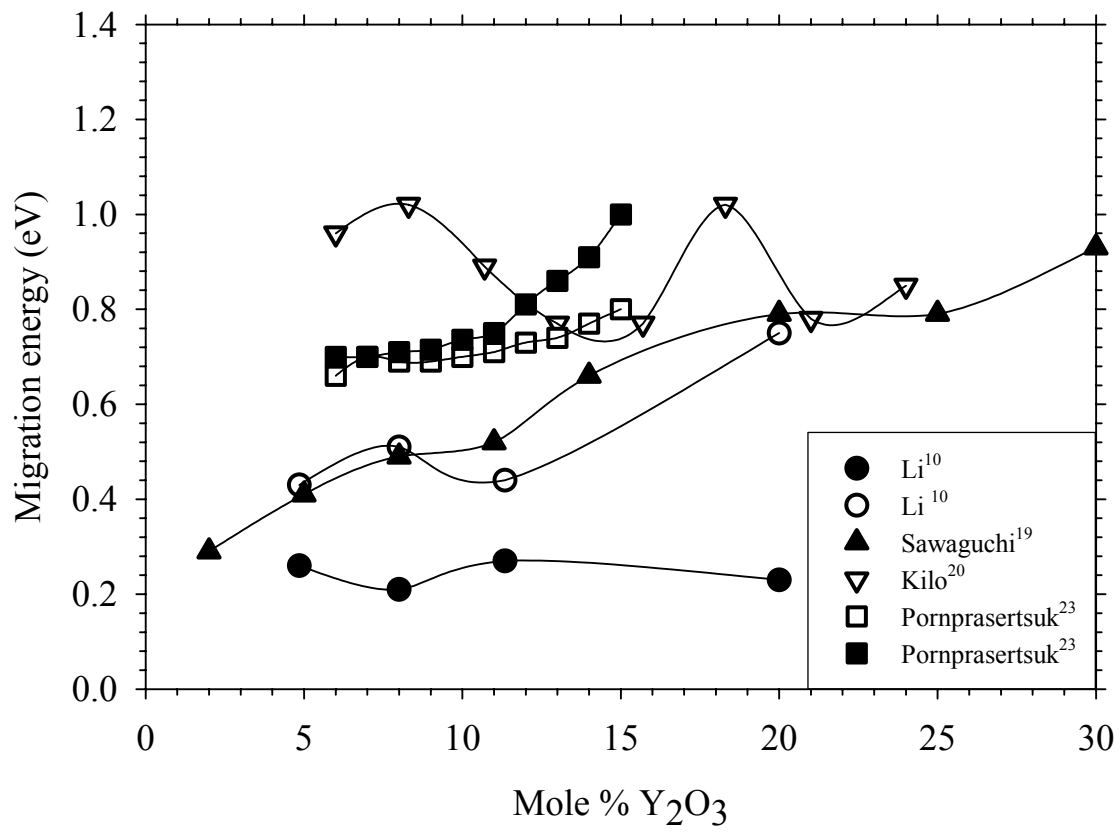Fig. 1   R. Devanathan, W. J. Weber, S. C. Singhal, J. D. Gale

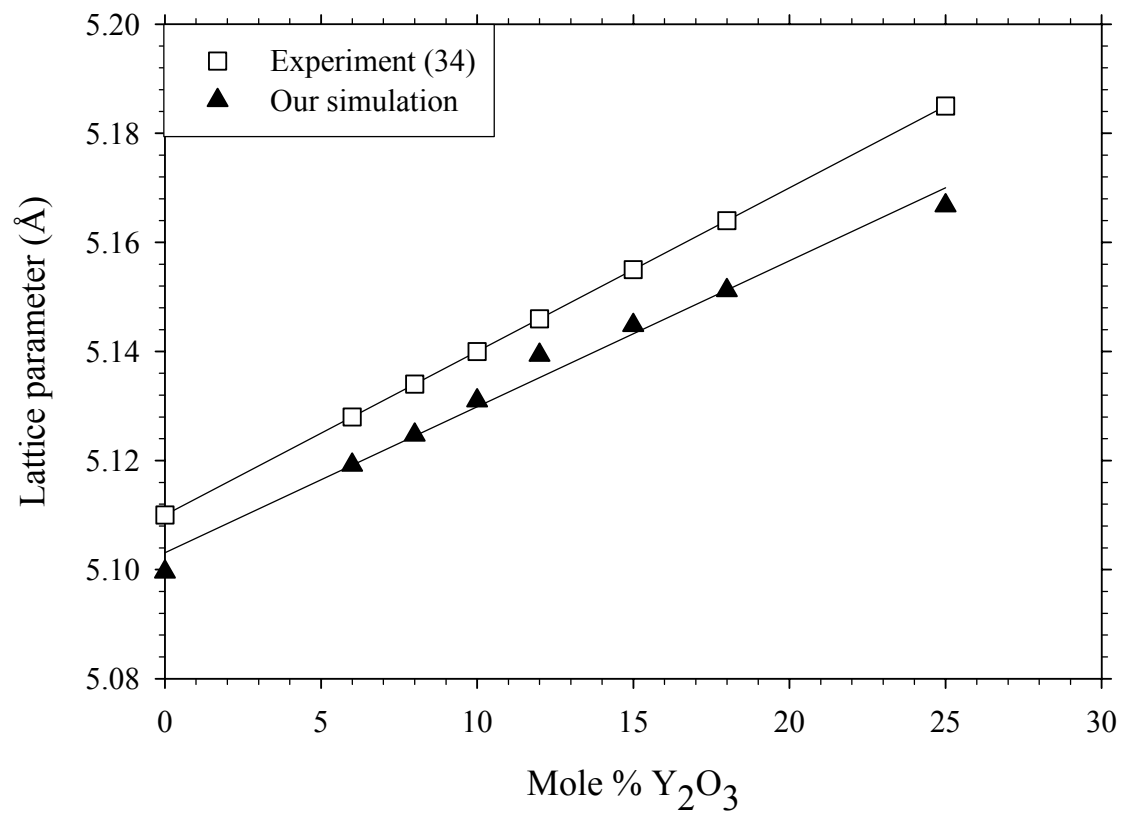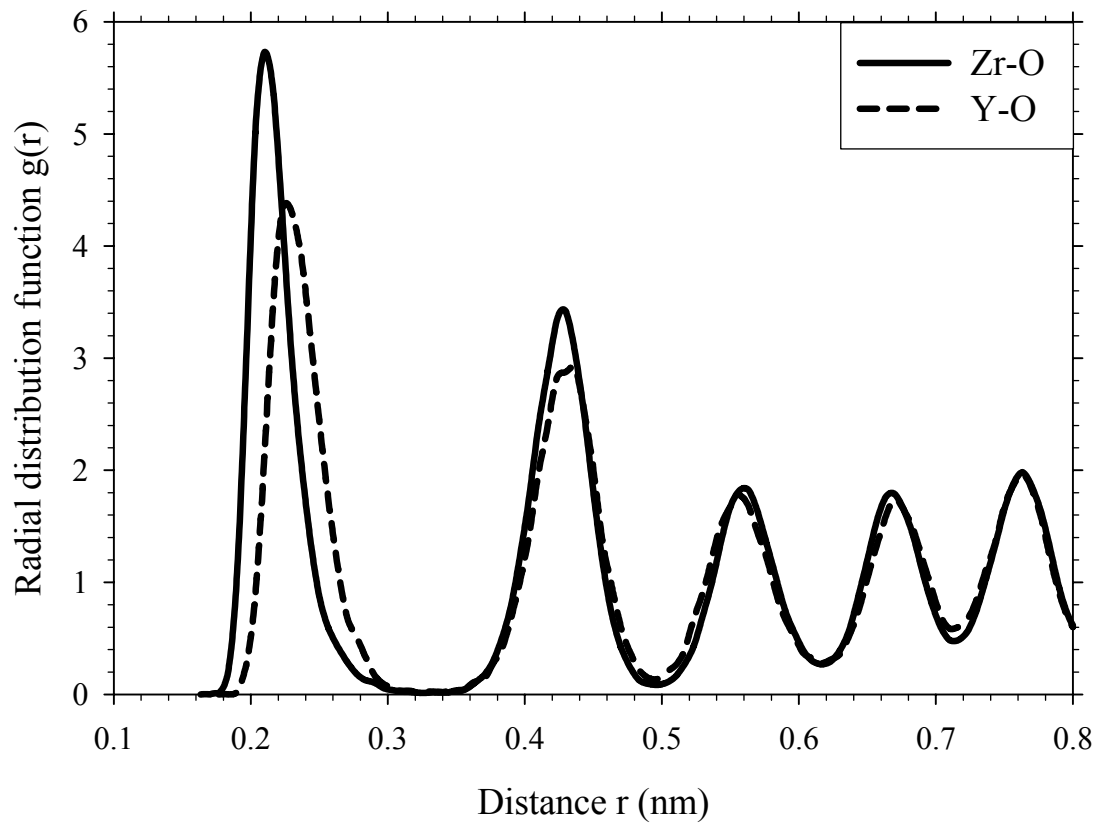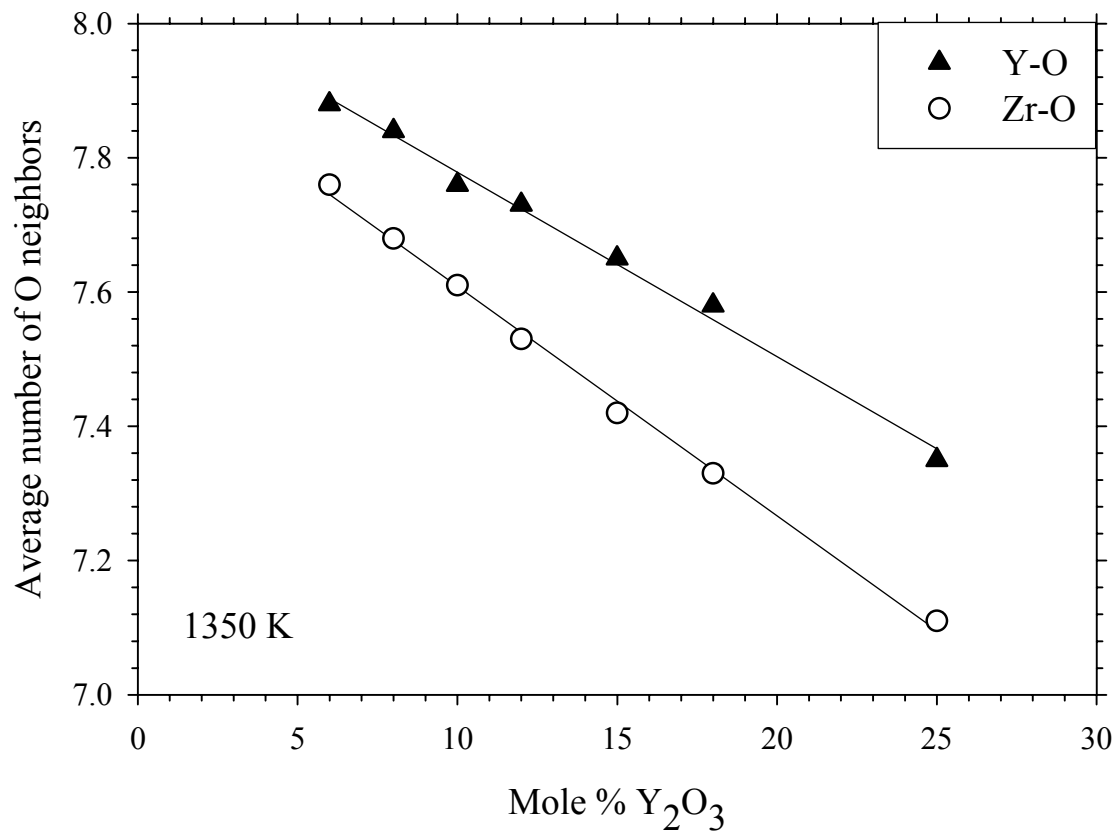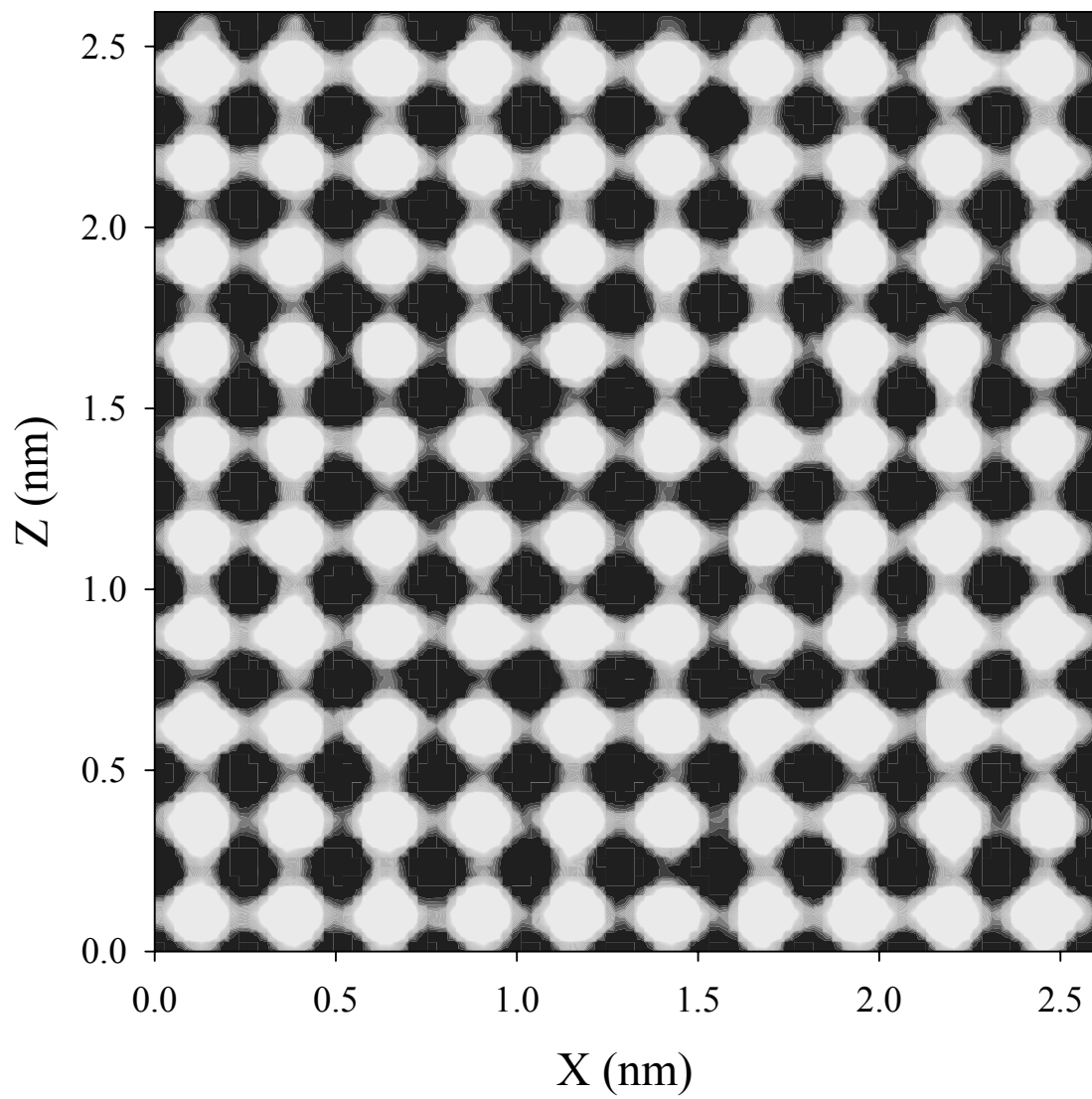Fig. 2   R. Devanathan, W. J. Weber, S. C. Singhal, J. D. Gale

Fig. 3   R. Devanathan, W. J. Weber, S. C. Singhal, J. D. Gale

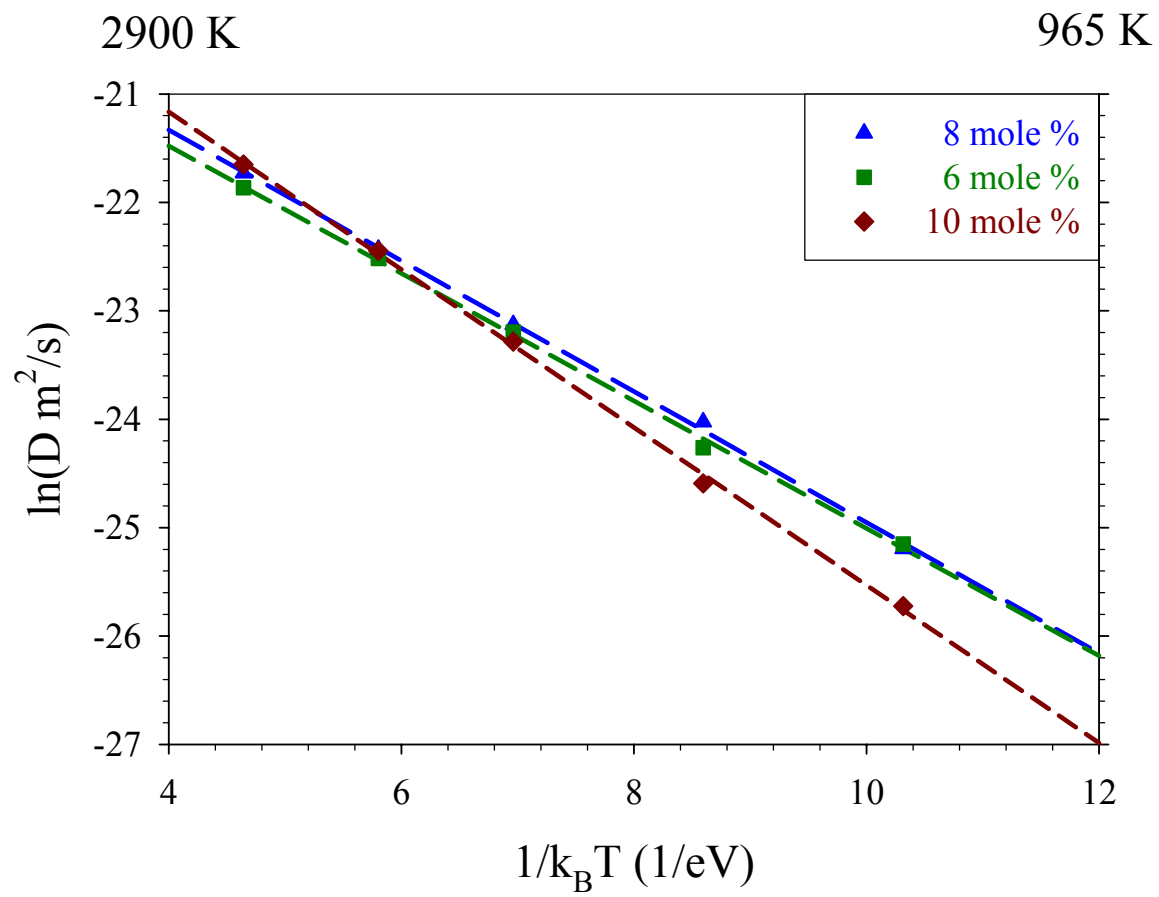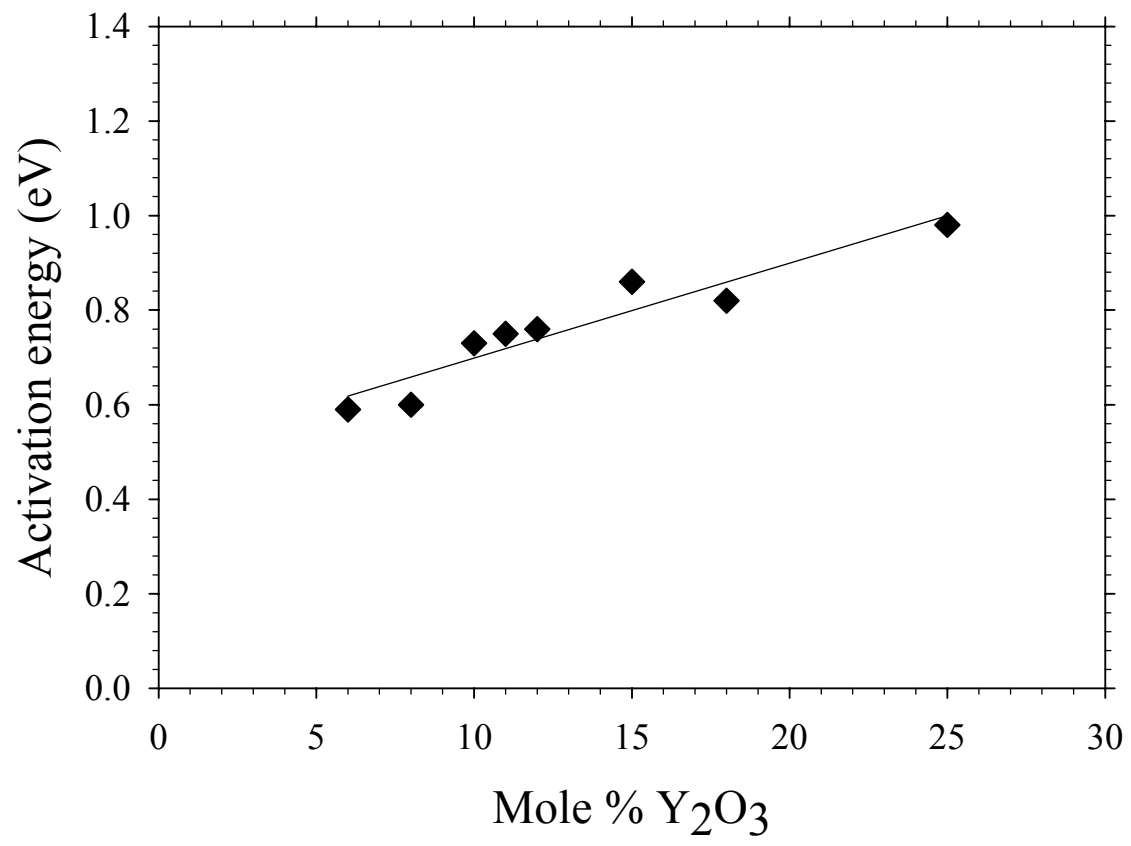Fig. 4   R. Devanathan, W. J. Weber, S. C. Singhal, J. D. Gale

Fig. 5   R. Devanathan, W. J. Weber, S. C. Singhal, J. D. Gale

Fig. 6   R. Devanathan, W. J. Weber, S. C. Singhal, J. D. Gale

Fig. 7   R. Devanathan, W. J. Weber, S. C. Singhal, J. D. Gale

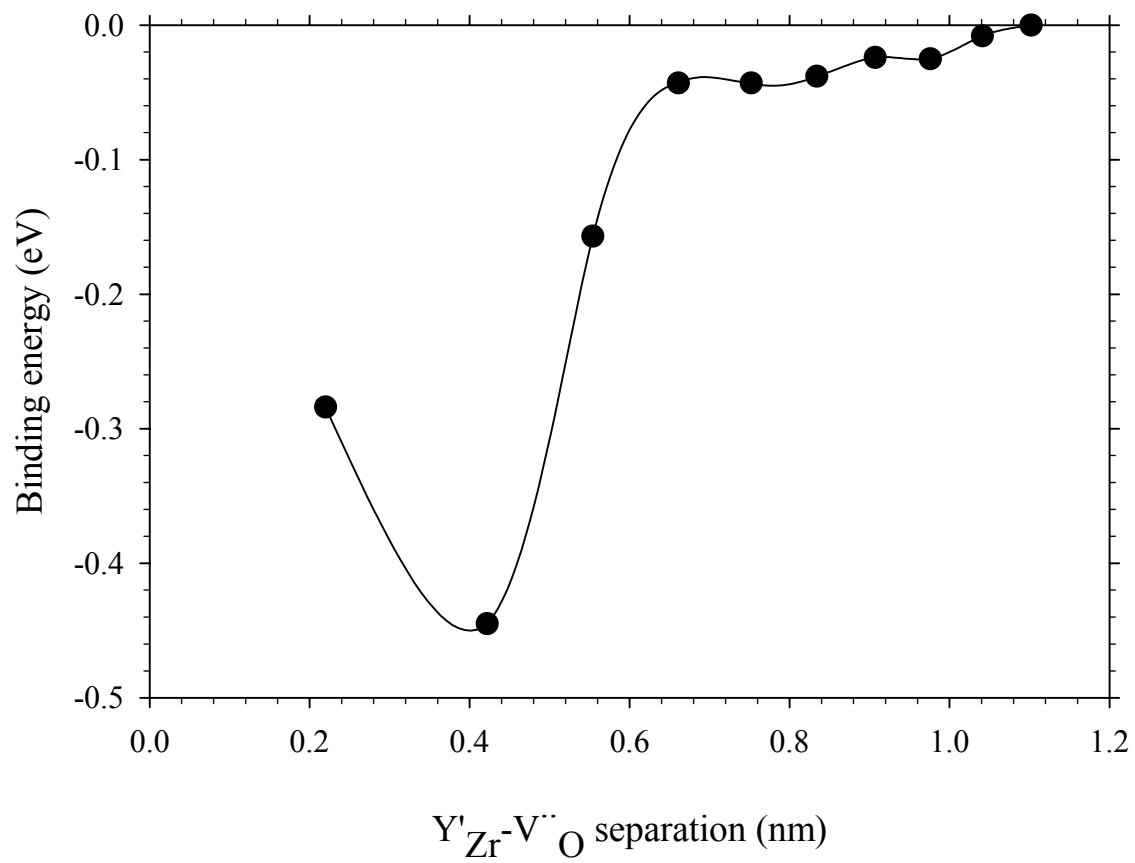Fig. 8   R. Devanathan, W. J. Weber, S. C. Singhal, J. D. Gale

Binding energy (eV) vs Y'$_{Zr}$-V$^{..}_O$ separation (nm)

Fig. 9 R. Devanathan, W. J. Weber, S. C. Singhal, J. D. Gale
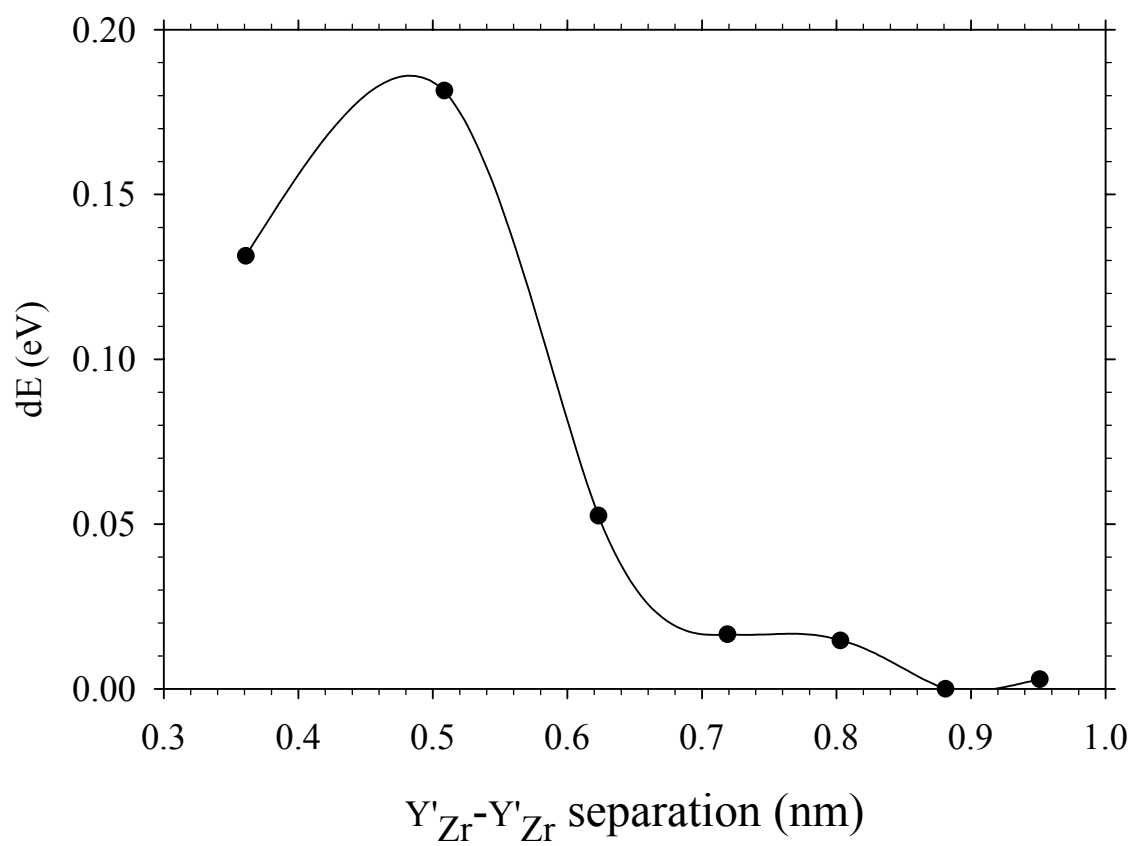
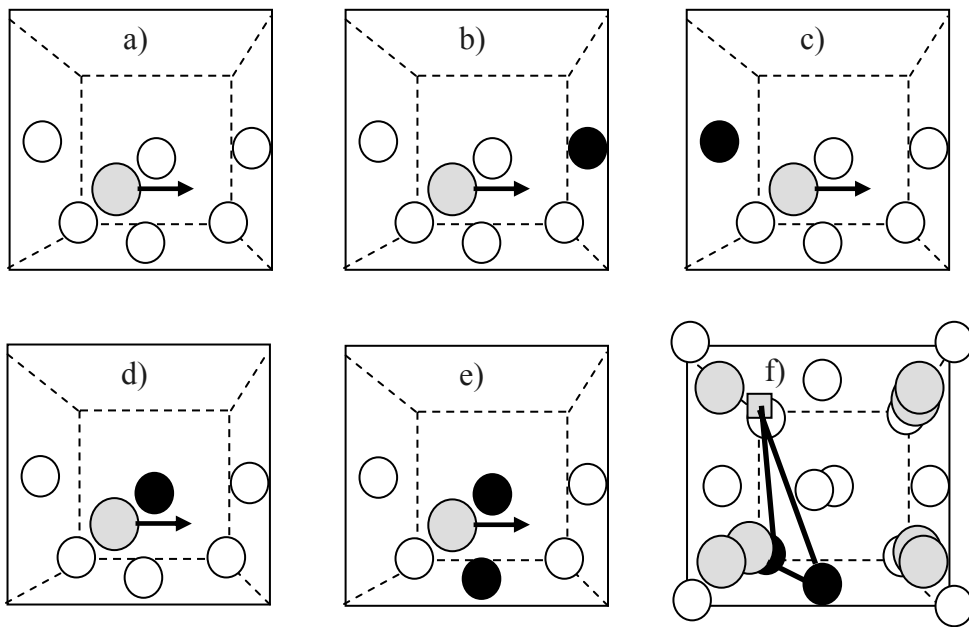Fig. 10   R. Devanathan, W. J. Weber, S. C. Singhal, J. D. Gale

Fig. 11   R. Devanathan, W. J. Weber, S. C. Singhal, J. D. Gale